Cement and Concrete Research 133 (2020) 106067

Contents lists available at ScienceDirect

Cement and Concrete Research

journal homepage: www.elsevier.com/locate/cemconres

Tensile response of UHPFRC under very low strain rates and low temperatures

Mohamed Abdul Hafiz*, Emmanuel Denarié

Laboratory of Maintenance and Safety of Structures, MCS-IIC-ENAC, EPFL - Ecole Polytechnique Fédérale de Lausanne, CH–1015 Lausanne, Switzerland

ARTICLE INFO

Keywords:
SH-UHPFRC
Tensile response
Very low strain rates
Temperature
SCM
Viscosity
Elastic limit
Acoustic emission

ABSTRACT

This paper addresses the uniaxial tensile response of Strain Hardening Ultra High-Performance Fiber Reinforced Concretes (SH-UHPFRC) subjected to very low strain rates and low temperatures. The influence of four different strain rates; 1×10^{-5}, 1×10^{-7}, 1×10^{-8} and 5×10^{-9} 1/s on the tensile properties like elastic limit, elastic modulus, tensile strength and the strain at tensile strength, was studied for two types of SH-UHPFRC mixes; Mix I with type I cement and silica fume, and Mix II with silica fume and 50% mass replacement of type I cement with limestone filler, at three curing temperatures; 20 °C, 10 °C and 5 °C. The tests at strain rates lesser than 1×10^{-6} 1/s are the first of their kind for UHPFRC materials and the results show a considerable impact on the elastic limit of the mixes. Acoustic Emission tests were also carried out for validation of test results of the elastic limit.

1. Introduction

Ultra High-Performance Fiber Reinforced Concretes (UHPFRC) are special types of cementitious materials reinforced with short discontinuous steel fibers, which exhibit a high tensile strength (over 12 MPa) and a significant strain hardening (1–5‰) for the best mixes, depending on the different fiber orientation situations encountered in practice. They also have a very low permeability and outstanding durability, making them very good materials for rehabilitation or reinforcement applications (combined with rebars), for the improvement of load carrying capacity and protective functions of existing structures [1].

This paper addresses the strain rate sensitivity of the tensile mechanical properties of UHPFRC and the associated literature. It is well known that the tensile properties like the elastic limit, f_{Ute} (also often referred to as first cracking stress, pre cracking strength), strain at the elastic limit ε_{Ute}, elastic modulus E_{mod}, tensile strength f_{Utu} and the strain at the tensile strength ε_{Utu} are all sensitive to the rate of application of load. In literature, the effect of strain rates is usually described using the Dynamic Increase Factor (DIF), which is the ratio of value of the property of the material at a dynamic strain rate with respect to that at a quasi-static strain rate. The CEB model code [2] recommends a reference quasi-static strain rate of 3×10^{-6} s^{-1} for the calculation of the DIF.

A schematic diagram showing the tensile response of SH-UHPFRC is shown in Fig. 1, which can be divided into three main domains;

1. Elastic domain: the region from the beginning until the elastic limit.
2. Hardening domain: the region from the elastic limit until the tensile strength.
3. Softening domain: the region from the tensile strength until full separation of the specimen.

The focus of the present study, was on the elastic and hardening domains and the effect of very low strain rates on the mechanical properties in these domains were investigated. In the elastic region, the elastic limit (f_{Ute}) as well as the elastic modulus in tension (E_{mod}) were studied whereas in the hardening domain, the tensile strength (f_{Utu}) and the strain at tensile strength (ε_{Utu}) were investigated. The f_{Ute} is the stress level until which the tensile stresses are proportional to the strains, with the corresponding strain given by ε_{Ute}. The slope of the stress strain curve in the elastic domain is given by the elastic modulus E_{mod}. The f_{Utu} and ε_{Utu} correspond to the coordinates of the peak stress in the tensile response.

The kinetics of various mechanisms influence the tensile response of UHPFRC as shown in Fig. 2, which include ageing of the material (hydration of binders), early age volume changes like autogenous shrinkage, drying shrinkage and thermal deformations, viscoelastic phenomena like creep and relaxation, and damage phenomena including microcrack onset and growth. There is a complex interaction of these phenomena especially under very low strain rates making it challenging to separate the contributions of the individual mechanisms. The phenomenon of ageing is prevalent mainly in the younger material

* Corresponding author.
E-mail address: mahafiz8@gmail.com (M.A. Hafiz).

https://doi.org/10.1016/j.cemconres.2020.106067
Received 5 April 2019; Received in revised form 18 November 2019; Accepted 30 March 2020

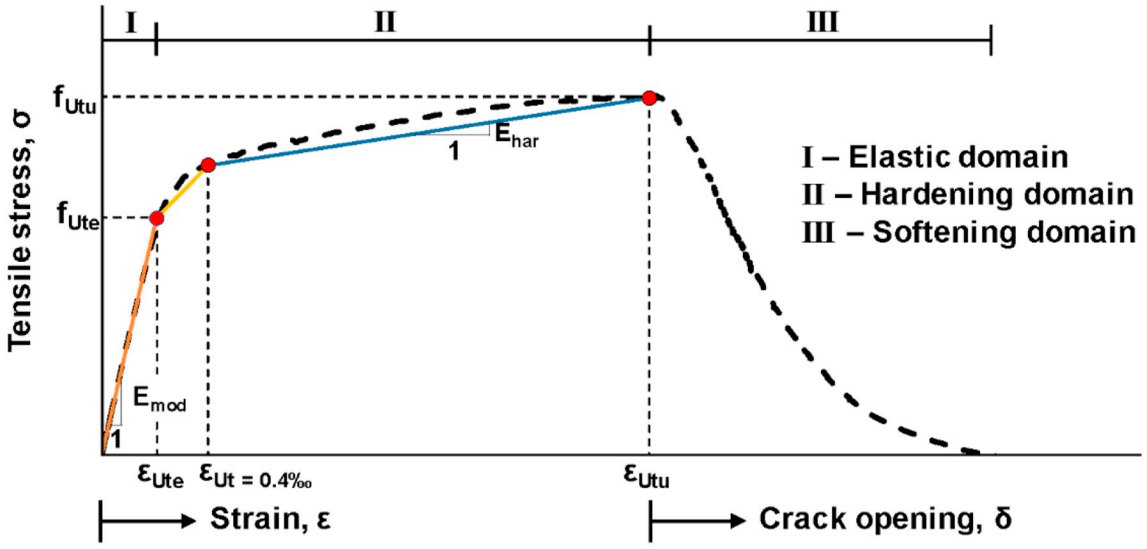

Fig. 1. Schematic tensile response of SH-UHPFRC.

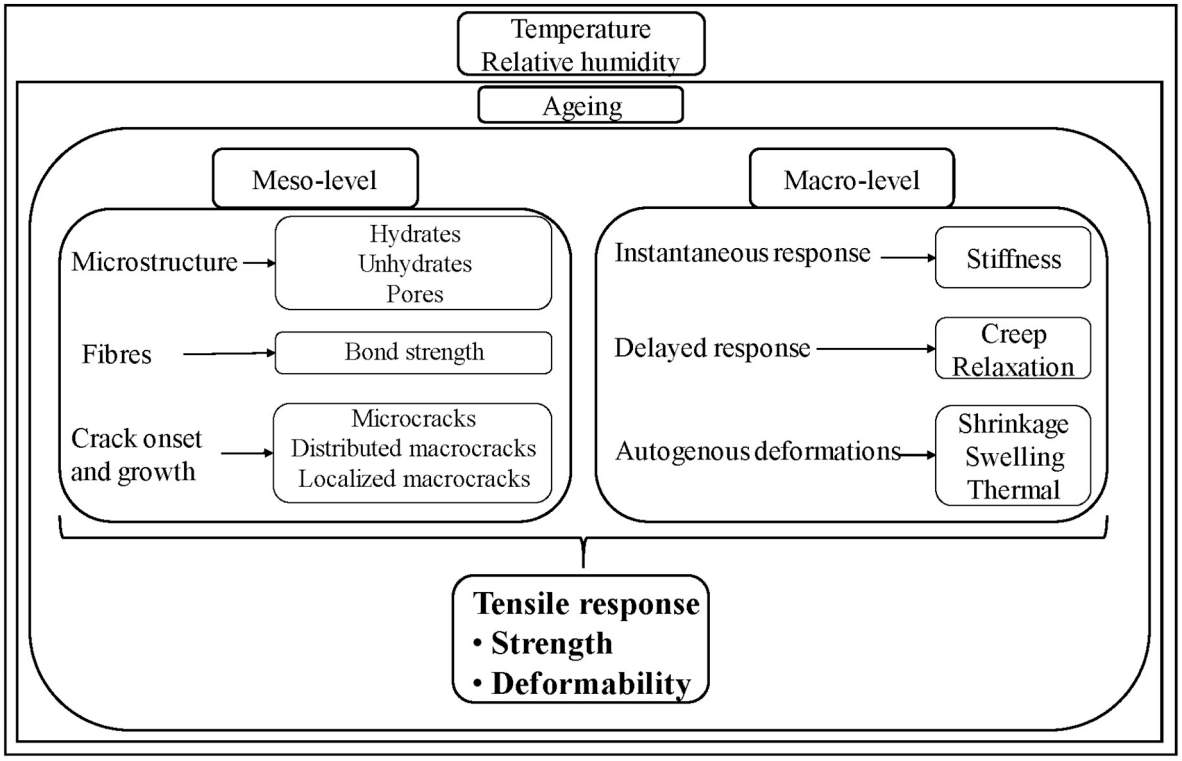

Fig. 2. Evolutionary mechanisms affecting the tensile response of UHPFRC.

(upto 3–5 days after addition of water), whereas in the long term, the influence of viscoelasticity and damage become dominant. These two phenomena, which produce similar effects (increased deformations and loss of stiffness), interact with each other depending on the stress level. On the one hand, for low strain rate, viscoelasticity plays an important role in the development of microcracks and crack propagation; whereas on the other hand, at high stress levels, the presence of microcracks lead to the development of non-linear viscoelasticity.

Rusch [3] was the first to highlight the effect of time dependent phenomenon on the strength of concrete under compression (static fatigue). Similar effects were shown for concrete under bending and tension by [4–7]. Many authors have shown the effect of monotonic strain rate on the tensile properties of normal concrete, both at high strain rates (1/s to 200 s^{-1}) [8–11] and at low strain rates (1 × 10^{-7} s^{-1} to 1/s) [12–15]. All the studies showed that the tensile strength of normal concrete increases with an increase in the applied strain rate. [16] showed that direct tensile tests on concrete done by [17] at a strain rate of 3 × 10^{-7} s^{-1} showed a significant decrease in the tensile strength when compared to the quasi static strain rate of 3 × 10^{-6} s^{-1} as recommended by the CEB model code formulation for concrete in tension [2]. Similar trends were also shown for concrete in compression by [18] for very low monotonic strain rates < 1 × 10^{-6} s^{-1}.

Recent studies suggest that the DIF for UHPFRC differ from that of normal concrete [19]. Because of the very high strength and specific fracture energy of these materials, they are very suitable to resist impact loading caused by explosions, vehicle crashes and falling rocks

[20]. As such, majority of the studies on the effect of strain rate on the tensile mechanical properties of UHPFRC are concentrated to the dynamic domain (1×10^{-4} s^{-1} to 1×10^{2} s^{-1}) [20–36]. All of these works discuss the strain rate effect using the direct tension test except [21,30] who had conducted flexural bending tests and [27–29] who had used splitting tension tests to study the strain rate effects in the dynamic domain.

The main fields of application of SH-UHPFRC are the design of new structures and rehabilitation works, for the improvement of load carrying capacity and protective functions of existing structures. In the latter case, when a new layer of UHPFRC is applied on an existing structure, it is subjected to early age volume deformations such as autogenous shrinkage, thermal deformations and drying shrinkage in certain situations. These deformations are restrained to different extents, depending on the relative stiffness of the new layer and the existing substrate and depending on the boundary conditions of the support, leading to the development of tensile eigenstresses in the material. Furthermore, these restrained deformations take place at very low strain rates (1×10^{-8} 1/s – 1×10^{-11} 1/s). It is therefore essential to investigate the tensile response of UHPFRC materials at these very low strain rates. To the best of authors' knowledge, the smallest tensile strain rate that was studied for UHPFRC was 1×10^{-6} s^{-1} [20], and no works have been done until now to understand the effect of very low strain rates ($< 1 \times 10^{-6}$ s^{-1}) on the tensile behavior of UHPFRC.

At very low strain rates, the couplings between hydration, creep and damage become more dominant. Bazant et al. [37,38] showed the influence of ageing and hydration on the creep phenomenon. Rossi et al. [39] showed that the basic creep of concrete is highly correlated to the acoustic emission and propagation of microcracks, indicating that microcracks play a major role in the creep of concrete at high stress levels. The influence of stress level and microcracking on the relaxation response of concrete was also studied in [5,40,41], which showed a higher relaxation response along the failure envelope (non-linear) when compared to that at lower stress levels, confirming the interaction of damage and non-linear viscoelasticity at higher stress levels. More recently, for UHPFRC, [42–44] studied the interaction of ageing, early age volume changes, stress level and loading history. [45] showed that at an age of 46 h (13 h after setting), UHPFRC exhibited non-linear creep under a stress level of 30% whereas at an age of 72 h (39 h after setting) it exhibited linear creep at a stress level of 32%. Using incremental relaxation tests in a TSTM, [42] showed that at high stress levels of 60% and 90%, higher relative relaxations were observed indicating a non-linear viscoelastic response.

Furthermore, temperature influences the kinetics of hydration, ageing and viscoelastic behavior. There is a complex interaction between the effect of temperature on the ageing and creep response of cementitious materials. On the one hand, a higher temperature leads to a higher creep response; whereas on the other hand, a higher curing temperature would lead to a higher apparent age (maturity) of the material and consequently a lower creep response [46]. The effect of thermal curing and temperature on the development of autogenous shrinkage and creep deformations were shown in [47–52], while the effect of the same on the mechanical properties were shown in [45,51,53–55]. However, contrary to prefabrication, for cast on site applications of UHPFRC, the local climatological conditions govern. In addition, in winter conditions, the cast on site UHPFRC layers will be subjected to very low temperatures. It is very well known that at low temperatures, the development of hydration is much slower than at ordinary temperatures, and only a few works have been carried out to study the influence of low curing temperatures on the development of hydration and autogenous shrinkage in UHPFRC [44,46]. Therefore, fundamental knowledge regarding the tensile behavior of UHPFRC subjected to low curing temperatures is needed for their successful applications for repair and rehabilitation.

Finally, increasing focus is now being given to the use of Supplementary Cementitious Materials (SCM) in UHPFRC mixes in view of sustainability, to reduce the environmental impact of cement production. Because of the very low water/cement ratio in UHPFRC mixes with pure cement, a significant portion of the cement remain unhydrated and it could advantageously be replaced by inert fillers like limestone filler, fly ash etc. [46,53,56]. Depending on the water/cement ratio, many studies have shown that the degree of hydration of cement in UHPFRC mixes with pure cement is as low as 30% after 28 days [44,46,51]. The unhydrated cement and silica fume simply act as fillers (physical effect), and improve the compactness of the matrix at the micro level and thereby lead to the increase of the mechanical properties at the macro level. However, from a sustainability point of view, cement is a very costly material to be used as a filler; not only in terms of monetary cost but also in terms of the environmental impact. Cement industry accounts for around 5% of the global carbon dioxide (CO_2) emissions. The CO_2 emission is directly proportional to the cement content in the concrete mix; 900 kg of CO_2 are emitted during the manufacture of every ton of cement [57,58]. As such, lesser the cement content in the UHPFRC, lesser will be the impact on the environment. However, not many works have been carried out to investigate the tensile behavior of these type of low clinker UHPFRC mixes, especially under very low strain rates.

In this paper, the effect of very low strains on the tensile response of two types of UHPFRC was investigated; Mix I with pure type I cement, silica fume and steel fibers and Mix II with 50% replacement of cement with limestone filler and a similar steel fibrous mix. Uniaxial direct tensile tests were conducted at four different strain rates; 1×10^{-5} s^{-1}, 1×10^{-7} s^{-1}, 1×10^{-8} s^{-1} and 5×10^{-9} s^{-1}, and at three different curing temperatures; 20 °C, 10 °C and 5 °C.

2. Experimental

2.1. Material

Two types of SH-UHPFRC mixes were studied in this paper, both from the CEMTEC$_{multiscale}$© family. The CEMTEC$_{multiscale}$© mixes were initially developed at Laboratoire Central des Ponts et Chaussées (LCPC), France [59]. This material was optimized and modified in the framework of the research works held in MCS/EPFL for rehabilitation and strengthening of existing structures [60,61] to produce Mix I, which is a SH-UHPFRC of type CM22_TKK_b. The ultra-compact cementitious matrix is composed of cement (type CEM I 52.5 HTS from Le Teil, Lafarge), white microsilica (SEPR, BET = 14 m^2/g), superplasticizer (Cementol Zeta Super S from TKK, Slovenia) and water. The material has a very high content of paste to accommodate all the fibers and therefore exhibits excellent rheological properties in the fresh state even though the water/binder ratio is very low, 0.129.

Because of the very low degree of hydration of Mix I (30% after 28 days [62], 50% of the cement in Mix I could be replaced by two types of inert limestone fillers; Betoflow D® and Betocarb SL® (OMYA). Using the concepts of packing density optimization, the composition of the different components like the cement, limestone fillers and the silica fume was designed. The new mix, CM22_TKK_b_LF, will be designated as Mix II from here on in the paper. More details on the mix design of the Mix II could be found in [62].

Both mixes had a fibrous mix containing two types of steel fibers; microfibers and macrofibers, with a total dosage of 9% by volume. The microfibers (steel wool, from Gervois, France) had a semi-circular section with an average diameter of 0.04 mm and a length of 2–3 mm, and an irregular aspect ratio allowing a high adhesion with a cementitious matrix. The macrofibers were straight, with l_f = 10 mm, d_f = 0.2 mm, from Bekaert, Belgium. The materials exhibit a significant strain hardening behavior under tension (1–2‰) [63,64]. The detailed compositions of Mix I and II are given in Table 1 and the properties in the fresh state are given in Table 2. More details regarding the properties of the mixes in the hardened state, as well as the chemical compositions of the powders in the mixes could be found in [62].

Table 1
Compositions of Mix I and II.

Material	Mix I	Mix II
	[kg/m^3]	[kg/m^3]
Cement	1467.0	733.7
Silica fume	381.4	293.5
Limestone filler 1 (Betocarb SL®)	–	223.0
Limestone filler 2 (Betoflow D®)	–	510.6
Steel fibers (straight macro fibers; l_f = 10 mm, d_f = 0.2 mm and microfibers/steel wool)	706.5	706.5
Total water	225.8	217.9
Superplasticizer from TKK, Slovenia; Zementol zeta super S; polycarboxylate; 25% solid content; (total amount)	20.5	14.7

Table 2
Properties of Mix I and II in the fresh state (average value from 4 tests).

Property	Units	Mix I	Mix II
Workability (ASTM - spread after 25 blows)	mm	179	146
Specific weight	kg/m^3	2834	2695
Air content	%	3.2	4.7

2.2. Uniaxial tensile test

The uniaxial tensile test is a difficult test to perform for cementitious materials, both with and without fibers. However, the results obtained from the test give a direct and reliable estimate of the tensile mechanical properties and do not need any complex inverse analyses to obtain the same, as is the case with flexural tests. One of the main difficulties in performing the tensile test is the misalignment of the specimen in the test setup and the eccentricity that arises from it. Even if the alignment is perfect before the test, because of the micro and macro crack formations during the test, the eccentricities may arise again. In the present experimental campaign, the eccentricity was constantly monitored with the help of four LVDTs in two perpendicular planes as shown in Fig. 3. Special care was taken to see that the specimens were aligned in such a way that the bending stress due to possible eccentricity was < 0.6 MPa, at least in the elastic domain of the tensile response.

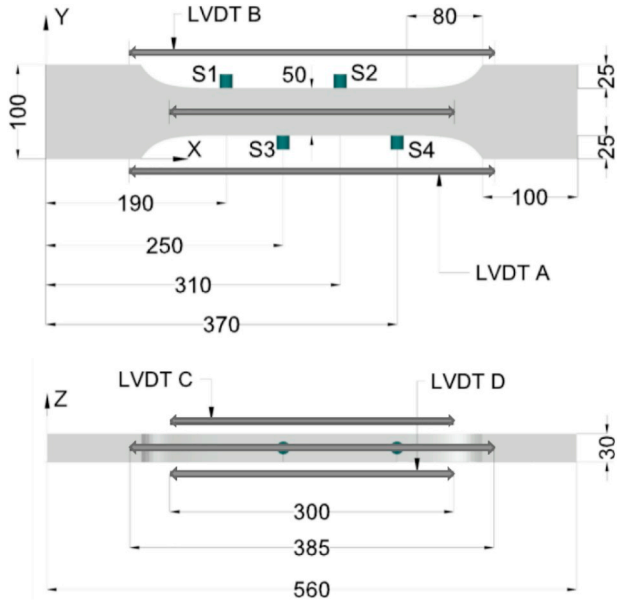

Fig. 3. Geometry of the dumbbell specimens, along with the positions of the LVDTs and the Acoustic Emission sensors S1, S2, S3 and S4 (all measurements are in mm).

Another major difficulty is the controlling of the gauge length. For strain controlled tests, if the fracture process zone occurs outside of the gauge length, it may not be possible to control the test anymore. This was minimized by selecting a gauge length of 385 mm, which even included the transition zone in the specimen, where there is a higher probability for crack formation. The boundary conditions of the test setup also play an important role in performing the tests. [65] has shown that fixed boundary conditions are less favorable for slight eccentricities compared to pinned end conditions, but lead to the only reliable estimation of the tensile response after the onset of cracking. As such, fixed boundary conditions were used for the tests in the present study.

2.3. Specimen shape and preparation

Specimens with dumbbell geometry were used for the study, the transition zone of which was designed using the Neuber's solution [66], which helped to minimize the stress concentrations around the necking. The geometry of the dumbbell specimen is shown in Fig. 3. The cross section in the middle straight portion of the specimen was 30 mm × 50 mm. Four LVDTs were placed on the specimen, with LVDT A and B in the XY plane and LVDT C and D in the XZ plane.

After the preparation of the UHPFRC mix, special attention was taken to cast the different specimens in a way as similar as possible from one specimen to the next, in order to avoid the scatter in the tensile responses due to the scatter in the fiber orientations between the individual specimens. The UHPFRC was guided into the molds with a half pipe, from one end and was slowly moved to the other end, so that the fibers follow the direction of flow of the mix and align themselves in the molds. Deformable tape was applied on the molds in the transition zones, to prevent the buildup of eigenstresses due to restrained shrinkage before demolding. Directly after casting, the specimens were kept in a climate chamber set at the required temperature of 20 °C, 10 °C or 5 °C. They were demolded two days later, but were continuously cured at the respective temperatures. Four circular aluminum discs of 100 mm diameter and 1.5 mm thickness were glued on the ends of the specimens for proper transfer of the loads through the grips. A system was developed to keep the circular plates on either side of the specimen parallel to each other and also to have the same thickness of glue between the four different circular plates and the specimen, thereby removing one possible cause for eccentricity while loading. The specimen was coated with a layer of paraffin wax to prevent drying shrinkage while curing.

2.4. Test setup and loading

The tests were carried out in an electromechanical testing machine, KAPPA 250 DS from ZWICK/ROELL with a capacity of 250 kN, with the test setup shown in Fig. 4. The testing machine was specially designed to carry out controlled tests at very low strain rates, as low as $1 \times 10^{-9}\ s^{-1}$. The boundary conditions were fixed at both ends of the specimen, without hinges before the grips. A cooling chamber was also attached along with the test setup to test the specimens under different curing temperatures; 20 °C, 10 °C and 5 °C. The tests were carried out at four different strain rates; $1 \times 10^{-5}\ s^{-1}$ (quasi static strain rate), $1 \times 10^{-7}\ s^{-1}$ (low strain rate), $1 \times 10^{-8}\ s^{-1}$ and $5 \times 10^{-9}\ s^{-1}$ (very low strain rates) for the two types of UHPFRC mixes; Mix I and Mix II, at an age of 14 days. The average of the displacements of LVDTs A and B was used to control the test and the strain rates were calculated using a gauge length of 385 mm.

2.5. Acoustic emission tests

An AMSY-6 acoustic emission system from Vallen Systeme was used for detecting the acoustic emission events. Preliminary tests were done

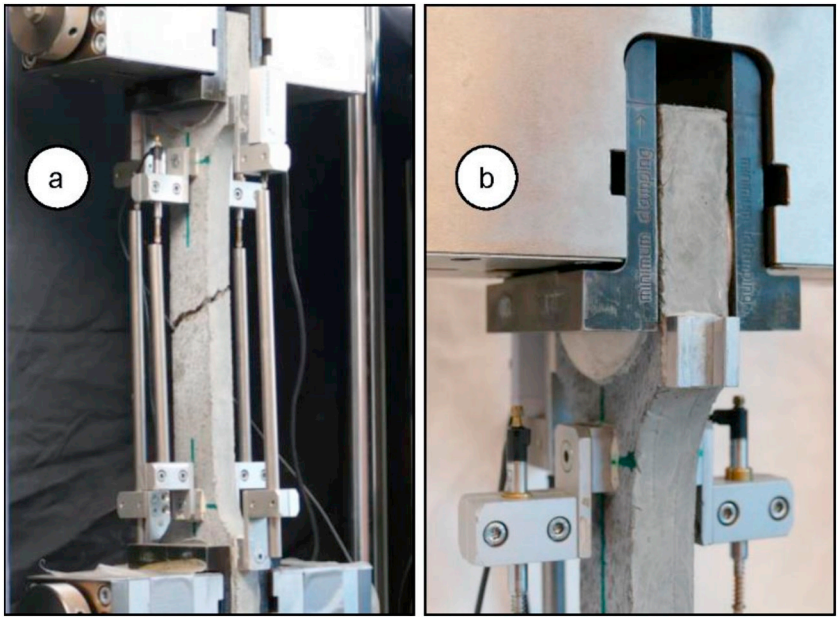

Fig. 4. a) Electromechanical KAPPA 250 DS test setup from ZWICK/ROELL with the dumbbell specimen for uniaxial tensile test, b) grips for fixed boundary conditions.

on an aluminum plate of the same geometry as that of the dumbbell specimens, for finding out the threshold of noise for the AE events, which were coming from the environment inside the lab as well as from the testing machine. After these tests, a threshold of 40 dB was set in the system as the noise threshold. The software VisualAE was used for the analysis of the obtained data and for the localization of the acoustic events in the specimen. The position of the sensors on the specimen is shown in Fig. 3.

3. Results and discussions

3.1. Overview of the tests

Table 3 shows the overview of the uniaxial tensile tests that were conducted under different configurations, with 90 tests in total. Fig. 5 shows the overall stress-displacement (average of LVDT A and B) curves from 3 different tests including the elastic, strain hardening and softening domains. Since the focus of the study was on the tensile parameters in the elastic and strain hardening domain, Fig. 6 shows the stress-displacement curves from all the tests under different configurations mainly in these two domains. The effect of the very low strain rates and low temperatures on the relevant mechanical properties will be discussed in detail in the coming sections.

Table 3
Overview of the uniaxial tensile tests.

UHPFRC Mix	Curing temperature (°C)	Name of the series	Strain rate (s^{-1})	Number of specimens tested
Mix I	20	M1 – 20C	1×10^{-5}	8
			1×10^{-7}	8
			1×10^{-8}	7
	5	M1 – 5C	1×10^{-5}	5
			1×10^{-7}	5
			5×10^{-9}	5
Mix II	20	M2 – 20C	1×10^{-5}	13
			1×10^{-7}	6
			1×10^{-8}	3
			5×10^{-9}	3
	10	M2 – 10C	1×10^{-5}	4
			1×10^{-7}	4
			5×10^{-9}	4
	5	M2 – 5C	1×10^{-5}	4
			1×10^{-7}	5
			5×10^{-9}	6

3.2. Effect of very low strain rates

3.2.1. Elastic limit

The elastic limit or the first cracking strength, f_{Ute} corresponds to the transition from the elastic behavior to the strain hardening behavior. It roughly corresponds to the strength of the matrix, even though some authors have shown that the fiber geometry or the fiber volume would affect the same [32,67]. For normal concrete without fibers, the elastic limit can be considered as the same as the tensile strength. For strain hardening cementitious materials, the accurate determination of the elastic limit is a very challenging problem. Different authors discuss different methods for obtaining the elastic limit of UHPFRC materials. In the present paper, the inverse analysis procedure described in SIA 2052 standard for UHPFRC [68,69] was followed for the determination of the elastic limit.

The procedure is graphically explained in Fig. 7 for a specimen MixI-SR12-S1 at a strain rate of 1×10^{-5} 1/s at 20 °C. From point 1 very close to the beginning on the stress-strain curve, the secant modulus of elasticity at point 2 corresponding to a stress level of 2 MPa was calculated. The calculated secant modulus is shown as point 3 in the Fig. 7. The secant modulus from the same point 1, along the stress-strain curve was then followed until there is a 10% drop from the same at point 2, and the corresponding point is marked as point 4. The stress level on the stress-strain curve corresponding to the point 4 is chosen as the elastic limit of the material [69].

Fig. 8 shows the average elastic limit calculated using the above procedure, for all the tests, along with the value of one standard deviation. The figure clearly shows that the elastic limit for both mixes decrease with the decrease in the strain rate. The trend is similar to what has been reported by many authors for quasi static to dynamic domain for concrete [8–11,13,14,17,70], for UHPFRC [20,32,35,36] and for similar materials like HPFRCC [71] and HSHDC [33]. In the present study, at the respective very low strain rates, the drop in the elastic limit from that at quasi-static strain rate was found to be 22%, 19%, 28%, 22% and 22% respectively for M1–20C, M1–5C, M2–20C, M2–10C and M2–5C. It can be clearly seen that the drop is significant,

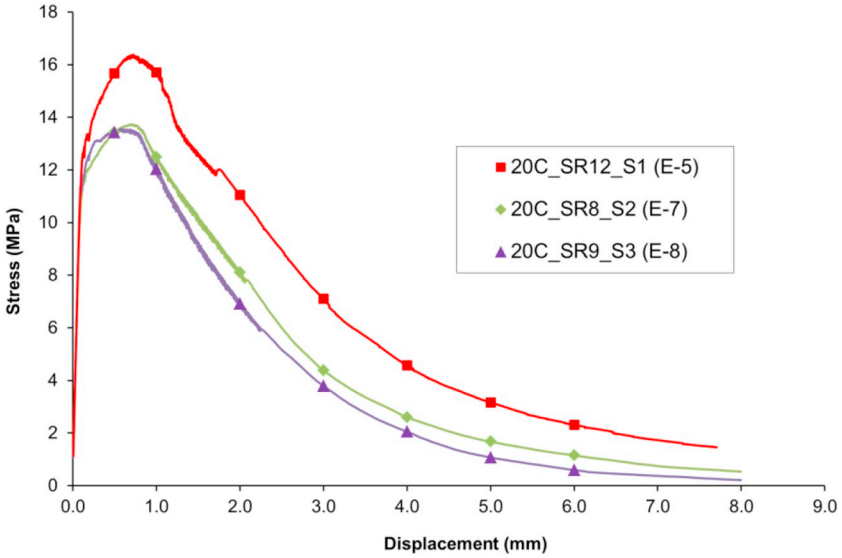

Fig. 5. Overall tensile response of three different tensile specimens at three different strain rates (1×10^{-5} 1/s, 1×10^{-7} 1/s and 1×10^{-8} 1/s) including the elastic, strain hardening and strain softening domain.

with its value being consistent between 19%–28%.

3.2.2. Elastic limit detection using acoustic emission measurements

One of the main aims of the acoustic emission technique in this study was to validate the procedure adopted for finding the elastic limit. Fig. 9a shows the cumulative AE events in a specimen Mix I-20C-SR13-S1 loaded at a strain rate of $1 \times 10^{-5}\ s^{-1}$ and Fig. 9b shows the same in a specimen Mix I-20C-SR13-S2 loaded at a strain rate of $1 \times 10^{-7}\ s^{-1}$. In both figures, corresponding to the elastic limit which has been determined using the procedure described in Section 3.2.1 [68,69], there is a sudden change in the rate of development of AE events. This clearly indicates that an objective threshold has been reached that can be characterized as elastic limit, and that microcracking is occurring at a faster rate from this point.

However, it should be noted that there are some acoustic events even before this point, thereby indicating that slight microcracking may occur even before the elastic limit. However, these microcracks were rather isolated as shown in Fig. 10 and therefore the specimen can still be considered to behave as an elastic material. Another important observation is that the AE events started appearing at a stress level of about 74% of the elastic limit in the specimen loaded at a strain rate of $1 \times 10^{-5}\ s^{-1}$ whereas it appeared at a stress level of about 69% of the elastic limit for a strain rate of $1 \times 10^{-7}\ s^{-1}$.

Fig. 10 shows the development of the acoustic events in the tensile test of dumbbell specimen Mix I-20C-SR15-S1. Using the procedure described in Section 3.2.1, the elastic limit was found out and is marked as point 3, while the tensile strength is shown by the point 6. The localization of the acoustic events at 6 different stress levels in the tensile response of the UHPFRC is shown and it can be seen that at point 2 just before the elastic limit, the acoustic events are very negligible and isolated. However, after the elastic limit at point 4, there is a sudden increase in the AE activity, therefore indicating the progression of damage at a much faster rate. Fig. 10 also shows a uniform distribution of the acoustic events throughout the gauge length of the specimen, before crack localization at the tensile strength.

3.2.3. Elastic modulus

Fig. 11 shows the effect of low strain rates on the elastic modulus in tension of the UHPFRC Mix I and Mix II. It can be seen that no proper conclusion could be drawn from the trend of elastic modulus under the different strain rates. Even though except for Mix I at 20 °C, all the other series show a trend wherein the elastic modulus decrease as the strain rate decrease from $1 \times 10^{-5}\ s^{-1}$ to $1 \times 10^{-7}\ s^{-1}$, and then increase again as the strain rate decrease further, the scatter of results, especially for the strain rate of $5 \times 10^{-9}\ s^{-1}$, is huge. It therefore makes it difficult to comment on the effect of strain rate on the elastic modulus of these mixes. However, Fig. 12 showing the DIF of elastic moduli, shows that except for a few erroneous values at a strain rate of $5 \times 10^{-9}\ s^{-1}$, the other DIF values are very close to 1. This indicates that the elastic modulus of UHPFRC does not appear to be significantly influenced by strain rates for the investigated range.

However, this trend is in contrast to the findings of [72–75] for conventional concrete in the dynamic domain, who found out that the elastic modulus increased with increasing strain rate due to the viscosity of pore water. Even then, [74,75] found that the DIF of elastic modulus showed a very small increase when compared to that of the tensile strength of the concrete. They discussed that the aggregates, which play the major role in the Young's modulus of concrete, were not sensitive to the viscous effects. Therefore the strain rate sensitivity was much less for elastic modulus when compared to that of the tensile strength. Furthermore, for UHPFRC materials in the dynamic domain, [19,20,36] reported no strain rate sensitivity for the elastic modulus while [32] was not able to reach a conclusion on the same because of the huge scatter in the results. These findings were similar to that of the present study. Following the same discussion as in [74,75] regarding the negligible viscous response of aggregates in conventional concrete, it can be argued that the steel fibers are even less sensitive to the viscous effects, thereby completely removing the effect of strain rate. Moreover, [36] also attributes the unclear strain rate sensitivity of elastic modulus to the insignificant effect of pore water viscosity at very low w/c ratio and to the homogeneity of the UHPC matrix. Nevertheless, it could also be argued that the strain rates investigated in the present study were still not low enough to exhibit a considerable decrease in the elastic modulus, and that specimens if tested even below a strain rat of 1×10^{-9} 1/s, may exhibit a much more pronounced influence of viscosity and therefore a lesser elastic modulus.

3.2.4. Tensile strength

Fig. 13 summarizes the effect of strain rates on the f_{Utu} of the two mixes for various curing temperatures. There was no unique trend in the tensile strength as the strain rate decreased. Mix I at 20 °C showed a decrease in the tensile strength with a decrease in the strain rate whereas, Mix II at 10 °C and Mix II at 5 °C exhibited an increase in the tensile strength. A third trend was shown by Mix I at 5 °C and Mix II at

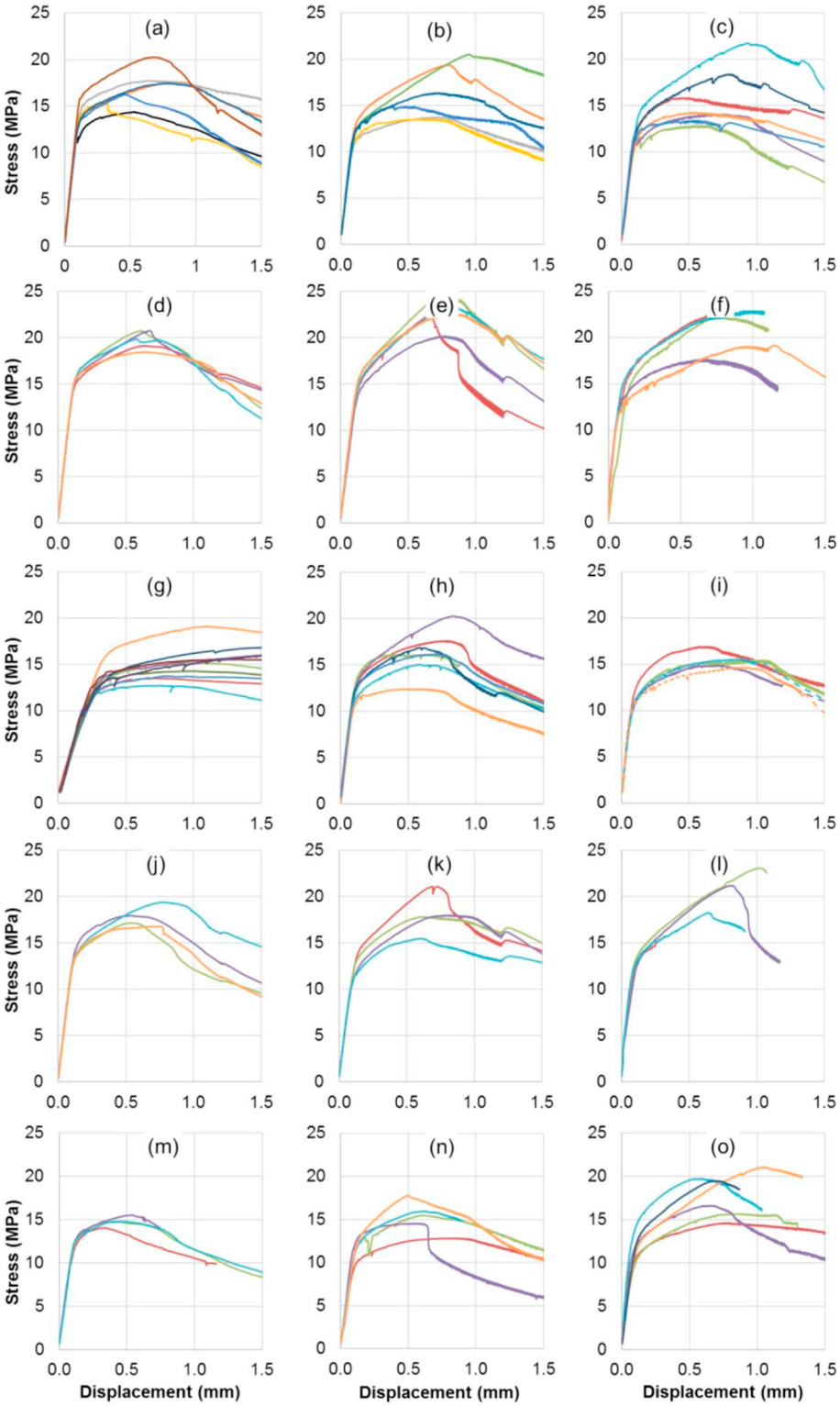

Fig. 6. Stress displacement curves for; a) M1-20C at 1×10^{-5} 1/s, b) M1-20C at 1×10^{-7} 1/s, c) M1-20C at 1×10^{-8} 1/s, d) M1-5C at 1×10^{-5} 1/s, e) M1-5C at 1×10^{-7} 1/s, f) M1-5C at 5×10^{-9} 1/s, g) M2-20C at 1×10^{-5} 1/s, h) M2-20C at 1×10^{-7} 1/s, i) M2-20C at 1×10^{-8} 1/s (dashed lines) and M2-20C at 5×10^{-9} 1/s (solid lines), j) M2-10C at 1×10^{-5} 1/s, k) M2-10C at 1×10^{-7} 1/s, l) M2-10C at 5×10^{-9} 1/s, m) M2-5C at 1×10^{-5} 1/s, n) M2-5C at 1×10^{-7} 1/s and o) M2-5C at 5×10^{-9} 1/s.

20 °C, with an initial increase and then a decrease in the tensile strength as the strain rates decreased. As such, no proper trend was seen for the effect of strain rate on the tensile strength of the mixes investigated. This is in contrast to the findings of the studies in the dynamic domain [20,22,23,31–33,35,36] where a clear dependence of tensile strength on the strain rate is reported with the tensile strength increasing with increase in the strain rate. On the other hand, as noted in [23,35], the increase in the DIF is quite steep in the dynamic domain (> 1/s), whereas it was much milder in the quasi-static domain. However, the lack of test data for strain rates lower than 1×10^{-6} s^{-1} for UHPFRC

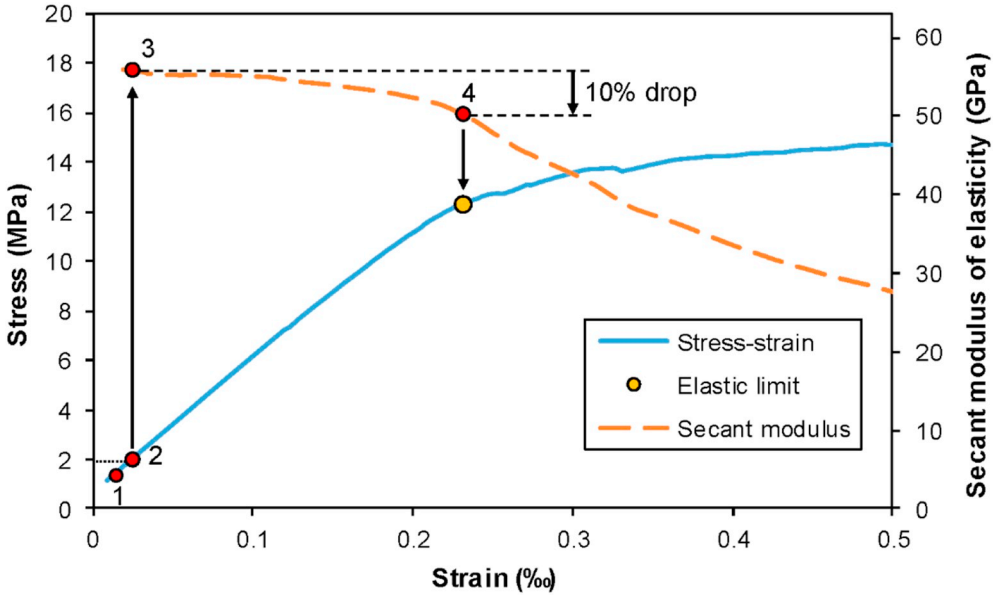

Fig. 7. graphical representation of the procedure for determining the elastic limit using the inverse analysis method (specimen MixI-SR12-S1, strain rate 1×10^{-5} 1/s at 20 °C).

materials, makes the comparison difficult and as a result, no trend in the tensile strength could be established. It could be assumed that the strain rate sensitivity becomes milder and milder as the strain rates decrease and ultimately reaches a state where the tensile strength is no more sensitive to the strain rate.

According to Naaman [76], the tensile strength of discontinuous fiber reinforced cementitious composites is given by Eq. (1), where λ is a factor which accounts for the average pullout length, fiber orientation effects and group reduction effects, τ is the bond strength of the fiber matrix interface, V_f is the fiber volume fraction and l_f/d_f is the aspect ratio of the fibers.

$$f_{Utu} = \lambda \tau V_f \left(\frac{l_f}{d_f}\right) \quad (1)$$

In Eq. (1), the only factor that is rate sensitive is the equivalent bond strength τ. As such, the strain rate sensitivity of the tensile strength very much depends on that of the pullout of fibers from the matrix. However, all studies on the effect of loading rates on the pullout behavior of high strength steel fibers embedded in UHPC matrix has been conducted for the dynamic domain [77–80]. [77] reported a comparatively smaller strain rate dependence of pullout load for straight smooth fibers when compared to that of hooked fibers. It could be argued that the effect becomes even smaller or negligible under very low loading rates, thereby making the bond strength and consequently the tensile strength rate insensitive. Moreover, [71,78] showed that the strain rate sensitivity of single fiber pullout decreased as the compressive strength of the matrix increased beyond 55 MPa. The very high compressive strength of the matrices in the present study could therefore make the pullout response strain insensitive for the range of strain rate investigated.

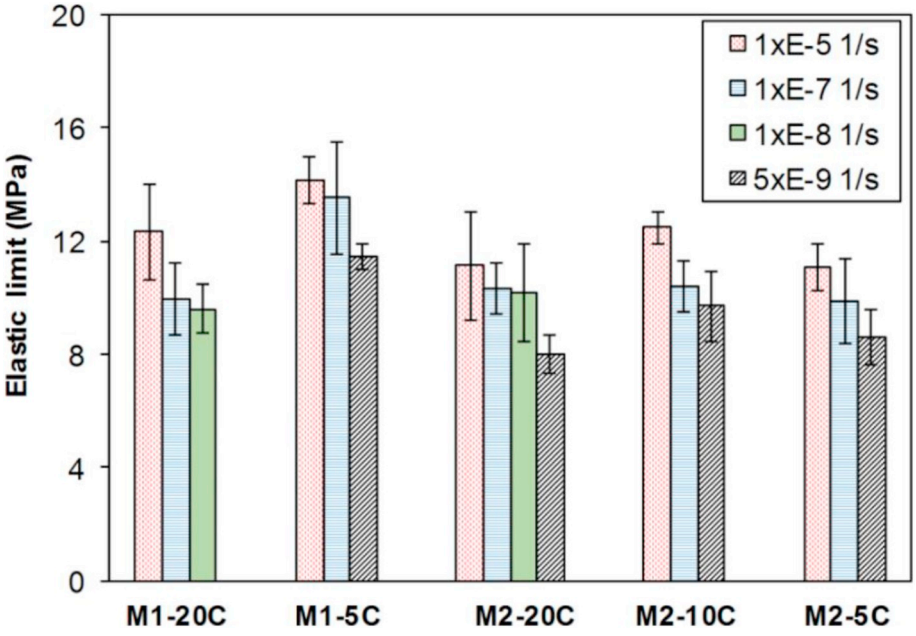

Fig. 8. Effect of strain rate on the elastic limit of Mix I and II.

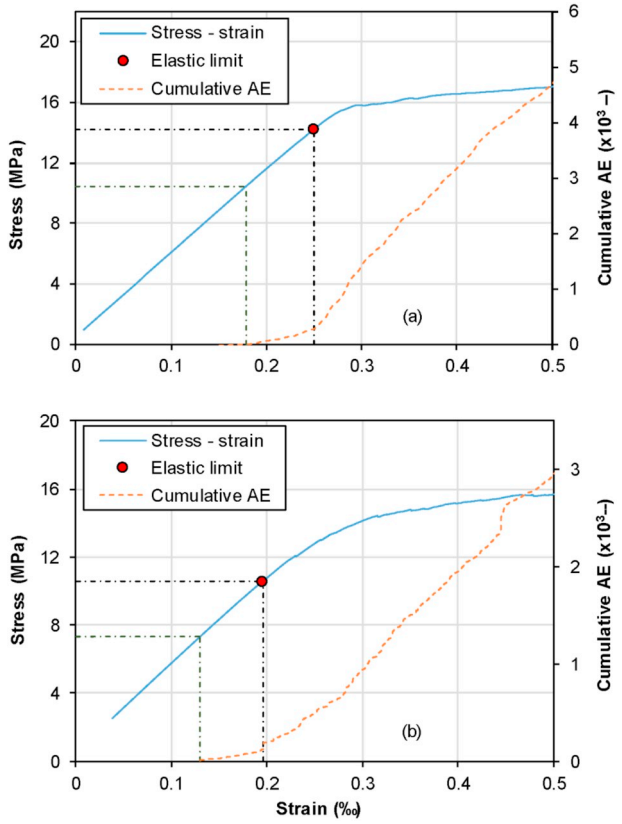

Fig. 9. Determination of the elastic limit using the 10% secant modulus drop method, along with the development of cumulative Acoustic Emission events at 20 °C, for a) specimen Mix I-20C-SR13-S1, strain rate of $1 \times 10^{-5}\ s^{-1}$, and b) specimen Mix I-20C-SR13-S2, strain rate of $1 \times 10^{-5}\ s^{-1}$.

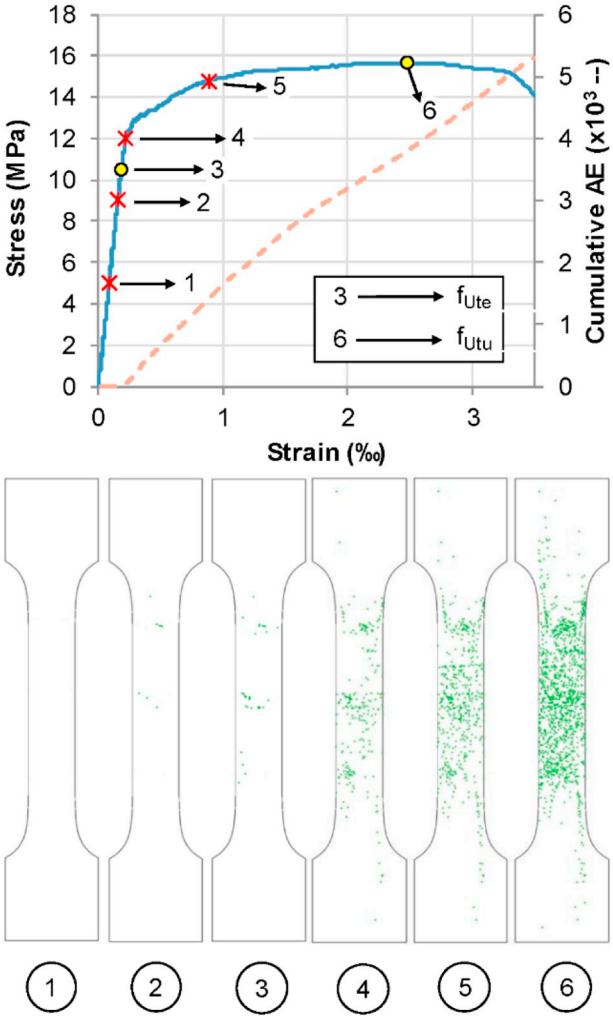

Fig. 10. Development of Acoustic Emission events at various stress levels during a uniaxial tensile test in a dumbbell specimen Mix I-20C-SR15-S1 at a strain rate of 1×10^{-5} 1/s at 20 °C.

If however, at very slow loading rates, the pullout of the single straight smooth fibers in the present study shows a strain rate sensitivity, it could be argued that the factor λ, including the effect of grouping of fibers or fiber orientation, counters the fiber pullout strain rate sensitivity, thereby making the overall composite action, strain rate insensitive. The results in [23,71] indicated a higher rate sensitivity of fiber pullout for mixes with lower fiber volume fraction, and the authors attributed this behavior to the group effect, wherein, the strain rate sensitivity is eliminated when a group of fibers interact together during pullout. The same effect may be present for the mixes in the present study as the fiber volume dosage is 9%. The scatter in the fiber orientation between individual specimens may also contribute to the scatter in the tensile strength [22], which can be another possible explanation for the strain rate insensitivity of the tensile strength, as seen in the present study. As such, it could be argued either that the strain rate insensitivity of tensile strength at very low strain rates, could be because of the strain rate insensitivity of the fiber pullout at these loading rates, or that the factors like fiber grouping and fiber orientation make the overall composite response strain rate insensitive.

3.2.5. Strain at tensile strength

Fig. 14 shows the trend of ε_{Utu} under varying strain rates for two mixes and three curing temperatures. Except for M1-20C at $1 \times 10^{-8}\ s^{-1}$ and M2–20C at $5 \times 10^{-9}\ s^{-1}$, one can notice an increase in ε_{Utu} with a decrease in the loading rates.

The trend is different from what many authors have reported for UHPFRC in the dynamic domain [23,24,31,32,35,36], wherein an increase in ε_{Utu} is reported with an increase in the strain rate of loading. The increase in ε_{Utu} was attributed mainly to the increase in the number of cracks within the gauge length as the strain rate increased [23,31]. However, [33] reported a decrease in the ε_{Utu} with an increase in the strain rate, similar to the findings in the present study. They showed that the average crack width decreased from 160 μm at 0.0001/s to 120 μm at 0.1/s, and attributed the same to the trend observed. Similar trend of decrease in ε_{Utu} with increasing strain rates were also observed by [81,82], who described it as the effect of fiber breakage at higher strains. In the present study, at very low strain rates, it could be argued that the observed trend is also dependent on the trends of f_{Ute} and f_{Utu} as discussed in Sections 3.2.1 and 3.2.4. Even though the f_{Ute} decreases with decrease in strain rate, the fibrous mix remains the same and therefore becomes more efficient in achieving strain hardening. Due to the lower f_{Ute} at very low strain rates, microcracks would have started to appear much earlier and as a result, the number of cracks until f_{Utu} could be much larger. Moreover, as shown by [33], the crack width would be larger at lower strain rates. These trends could therefore explain the trend of ε_{Utu} under very low strain rates in the present study.

3.3. Effect of low temperatures

3.3.1. Age vs maturity

Lower temperatures slow down the hydration reaction and ageing of the material. The Arrhenius equation and the apparent activation energy could be used to find out the maturity of the mixes to indicate the extent of hydration processes and its sensitivity to temperature. [46] found out the apparent activation energy for a UHPFRC mix CM22_TKK which was the predecessor of the Mix I in the present study. The value

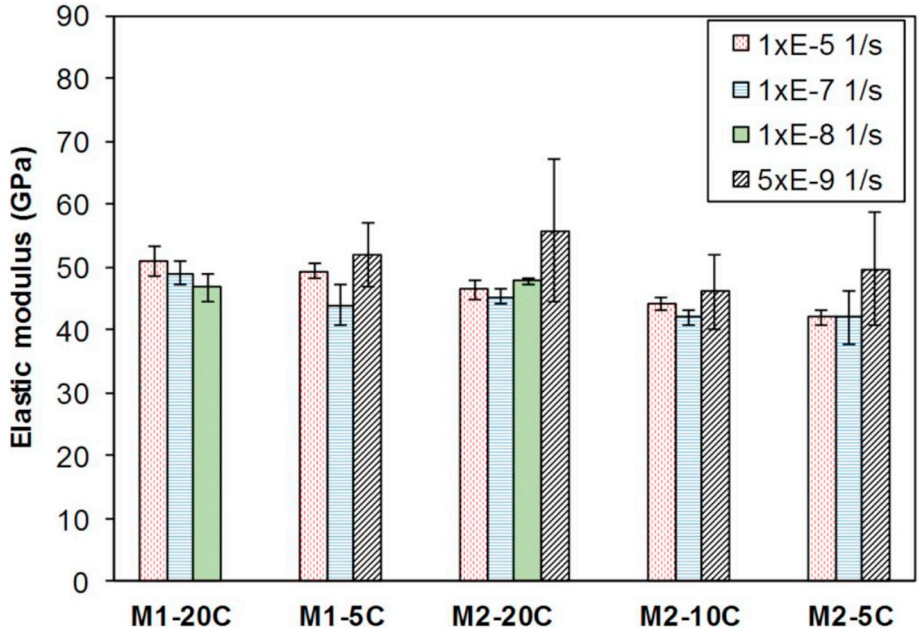

Fig. 11. Effect of strain rate on the elastic modulus in tension, of Mix I and II.

of $E_a/R = 3300$ K from that study [46], where E_a is the apparent activation energy in J/mol·K and R is the ideal gas constant, with a value of 8.314 J/mol·K, was assumed for the Mix I in the present case. For Mix II, a value of 4000 K was found out after conducting isothermal calorimetry tests at three different temperatures (not shown here). The maturity of the mixes corresponding to an age of 14 days is shown in Table 4.

3.3.2. Elastic limit

Fig. 15 shows the effect of temperature on the elastic limit for both the mixes under different strain rates. Mix I shows higher elastic limits at a temperature of 5 °C than at 20 °C, even though the maturity of the former is lesser than that of the latter. One possible explanation for this trend could be the denser microstructure under low temperatures, with significantly decreased quantity and size of capillary pores as indicated in [83]. Another possible explanation could be the crisscross effect seen in cumulative heat developed in isothermal calorimetry tests for similar UHPFRC mix under different temperatures as shown by [46]. It was seen that the cumulative heat developed at a temperature of 5 °C crossed that at 10 °C, at an age of approximately 10 days, but didn't cross that at 20 °C. It could be argued that at a later age for Mix I, the cumulative heat and consequently the hydration can be higher for a curing temperature of 5 °C, following similar discussion.

However for Mix II, the trend was slightly different as can be seen in Fig. 15, with a higher elastic limit at 10 °C, except at a strain rate of 1×10^{-7} 1/s. Nevertheless, this could be also be explained with the microstructure and crisscross effect, along with the development of hydration in Mix II. It was shown in [62] that the development of elastic modulus and hydration at 20 °C in Mix II was much slower than that of Mix I, and it took more time for Mix II to reach the final asymptotic

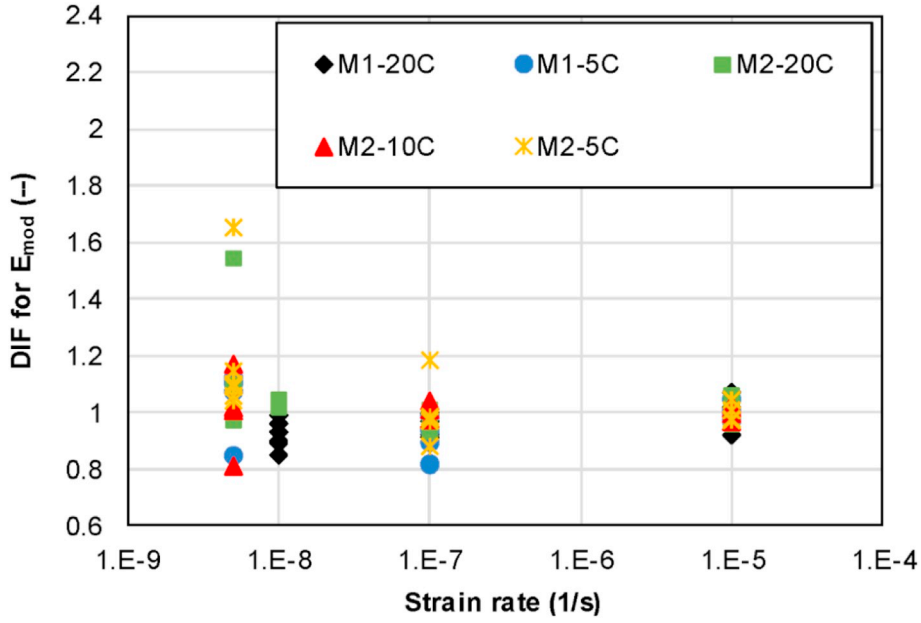

Fig. 12. DIF for elastic modulus in tension, of Mix I and II at very low loading rates.

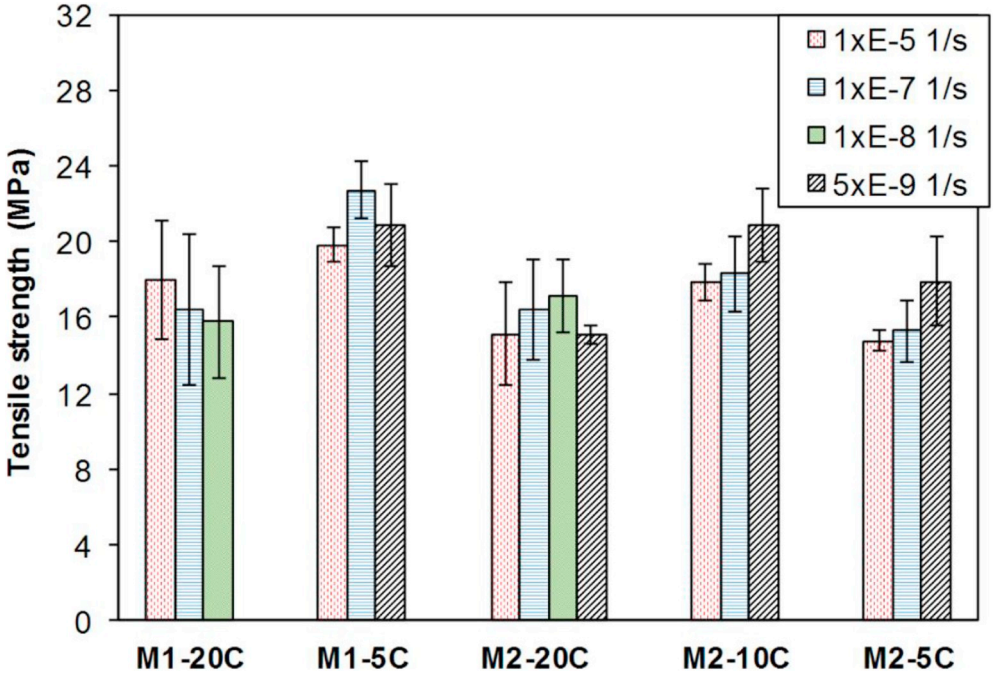

Fig. 13. Effect of strain rate on the tensile strength of Mix I and II.

value of elastic modulus or degree of hydration. As such, it may need more time to form the microstructure especially under lower temperatures, thereby delaying the two effects previously discussed. In Fig. 15, it could be argued that at 10 °C, the two effects have already occurred, thereby showing a higher elastic limit (except for strain rate of 1×10^{-7} 1/s), whereas it needs more time for the effects to be seen at 5 °C.

3.3.3. Tensile strength

Fig. 16 shows the effect of temperature on the tensile strength for both the mixes under different strain rates. It can be seen that the trend is very similar to that of the elastic limit. The behavior could therefore be attributed to the same effects as described in the case of f_{Ute}. A similar trend of higher tensile strength at lower temperatures was reported by [7] for steel fiber concrete. [84] showed that the pullout of single fibers from cement pastes with and without microsilica showed a higher bond stress at a temperature of 38 °C compared to that at 2 °C at 7 days, whereas the trend was inverted when tested at 90 days. The higher bond stress at lower temperatures can also be attributed to the better microstructure under these conditions.

3.3.4. Strain at tensile strength

Fig. 17 shows the effect of temperature on ε_{Utu} for the different configurations tested, in which no particular trends were seen. The

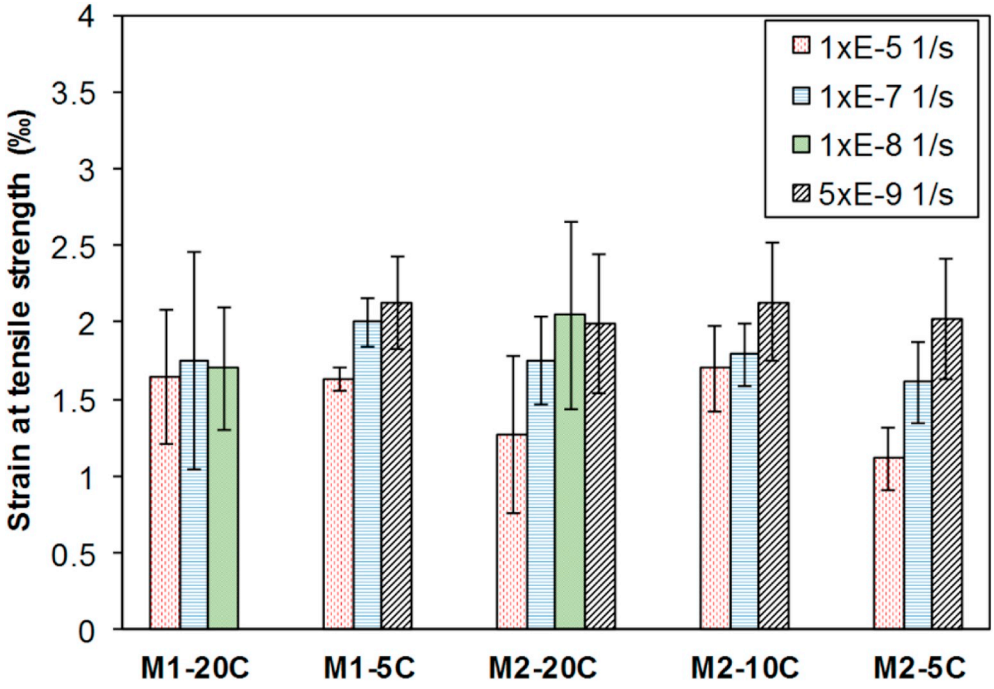

Fig. 14. Effect of strain rate on the strain at tensile strength of Mix I and II.

Table 4
Maturity at the time of testing under different temperatures.

Temperature	Age at the time of testing	Maturity at the time of testing for Mix I	Maturity at the time of testing for Mix II
°C	Hours (days)	Hours (days)	Hours (days)
20	336 (14)	336 (14)	336 (14)
10	336 (14)	226 (9.4)	207 (8.6)
5	336 (14)	183 (7.6)	161 (6.7)

complex interaction of creep and temperature as indicated earlier could be the reason for the observed independence. Moreover, the effects of fiber orientation and fiber grouping add to the complexity of the response making it apparently temperature independent in the present case.

4. Analytical models

4.1. Overview

The CEB model code [2] recommends a quasi-static strain rate of $3 \times 10^{-6}\ s^{-1}$ for the calculation of the DIF. However, not every studies on the effect of strain rate on the tensile response of UHPFRC or similar materials consider this as a quasi-static strain rate, but instead considers $1 \times 10^{-5}\ s^{-1}$ or $1 \times 10^{-6}\ s^{-1}$. This is not ideal for comparative and modelling purposes, but as pointed out in [19], the dynamic strength increase is minimal in this range of strain rates and therefore the DIF from different studies could be compared. As such, for the experimental tests in the present study, the DIF was calculated using a quasi-static strain rate of 1×10^{-5} 1/s. The DIF for the different tensile properties were compared with analytical models in the literature, the general format of which is shown in Eq. (2) [85].

$$DIFproperty = \begin{cases} \left(\frac{\dot{\varepsilon}}{\dot{\varepsilon}_s}\right)^{A*\delta}, \dot{\varepsilon} \le t\ s^{-1} \\ \beta\left(\frac{\dot{\varepsilon}}{\dot{\varepsilon}_s}\right)^{B}, \dot{\varepsilon} > t\ s^{-1} \end{cases} \quad (2)$$

where property refers to the relevant tensile property studied; A, B, β, δ are the parameters of the model and t refers to the strain rate in s^{-1} at which the transition occurs. In the following sections, existing analytical models along with new best fitting models will be used to analyze the DIF for f_{Ute} and ε_{Utu}. No models were developed for E_{mod} or f_{Utu} as these properties did not exhibit a clear strain rate sensitivity in the present study.

4.2. Effect of strain rate on f_{Ute}

The CEB model code parameters for f_{Ute} are given in Table 5, where f_c' is the quasi-static compressive strength and $f_{c,0}' = 10$ MPa. For the ease of comparison, it could be assumed that the elastic limit of fiber reinforced cementitious materials is the same as the tensile strength of the matrix, and therefore the CEB model could be used to compare the f_{Ute} of these materials. Malvar and Ross [16] compiled fifteen studies on the effect of strain rate on the tensile strength of conventional concrete at strain rates in the range of $1 \times 10^{-6}\ s^{-1}$ to $1 \times 10^{2}\ s^{-1}$ and formulated the model as shown in Table 5 for the prediction of the DIF. They used the same quasi-static strain rate as that of the CEB formulation.

Both the models were used to predict the DIF only until the quasi-static strain rate of $3 \times 10^{-6}\ s^{-1}$, at which the DIF value is 1. The tests in the present study are done at strain rates lower than this quasi-static strain rate. Using regression analysis, a new best fitting model similar to that of Eq. (2) has been proposed for the DIF of f_{Ute}. The model was developed only for strain rates $< 1 \times 10^{-5}\ s^{-1}$, and therefore includes only the first part of Eq. (2), the parameters of which are shown in Table 5. The quasi-static strain rate for the new model was chosen as the same as that of the other models for better comparison. It should be noted that the terminology of Dynamic Increase Factor is maintained, even though the factor is < 1 for lower strain rates.

Fig. 18 shows the predictions of the three models and the values of the calculated DIF for f_{Ute} from the five series of tensile tests in the present study. It can be seen that the CEB model as well as the Malvar and Ross model predict the response at low strain rates reasonably well, but a much higher drop in the elastic limit was seen in the tests as shown by the new best fitting model.

4.3. Effect of strain rate on ε_{Utu}

Many authors have reported the effect of strain rates in the dynamic

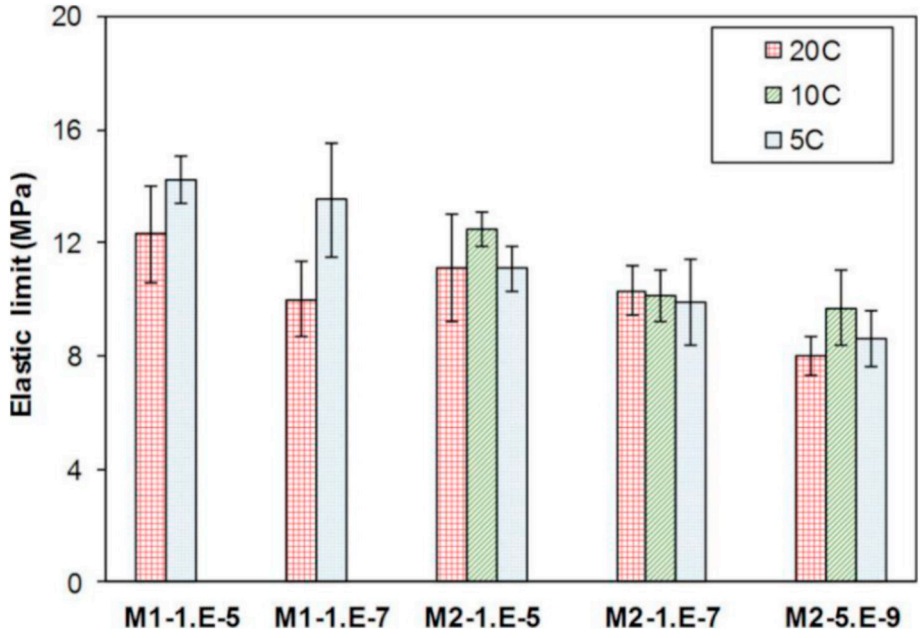

Fig. 15. Effect of temperature on the elastic limit for different mix type and loading rates [X-axis - "Mix type-strain rate (1/s)"].

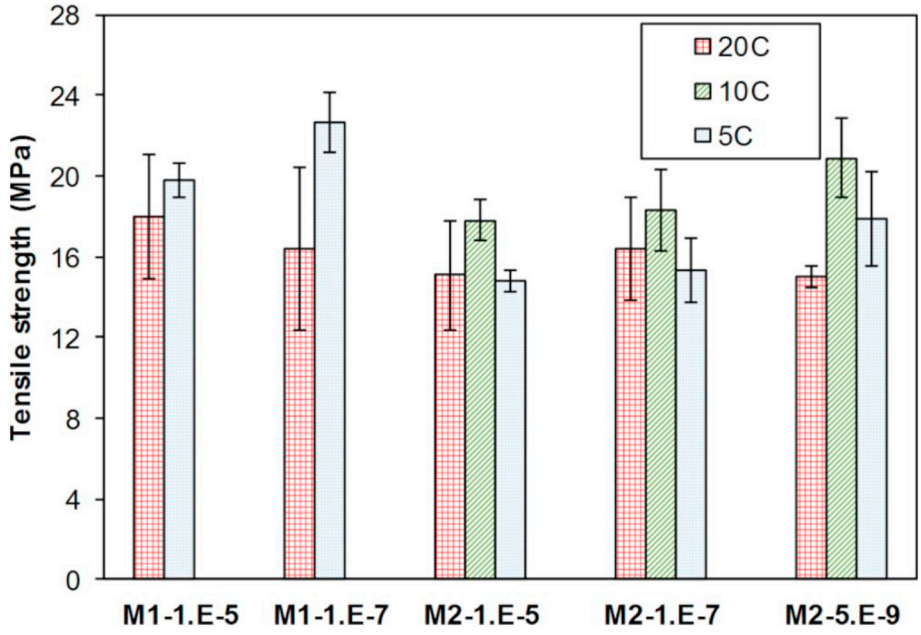

Fig. 16. Effect of temperature on the tensile strength for different mix type and loading rates [X-axis - "Mix type -strain rate (1/s)"].

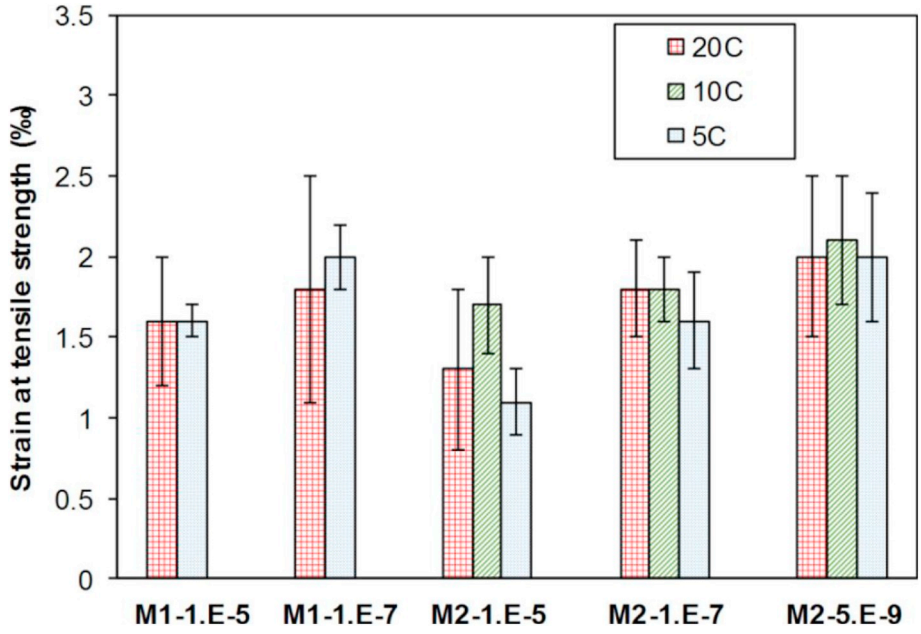

Fig. 17. Effect of temperature on the strain at tensile strength for different mix type and loading rates [X-axis - "Mix type-strain rate (1/s)"].

Table 5
Parameters of the analytical models for the prediction of effect of strain rate on the DIF for f_{Ute}.

Property	Model	$\dot{\varepsilon}_s$ (s^{-1})	A (–)	B (–)	β (–)	δ (–)	t (s^{-1})
$DIFf_{Ute}$	CEB [2]	3×10^{-6}	1.016	0.333	$\log\beta = 7.11\delta - 2.33$	$\delta = \frac{1}{10 + 6\frac{f'_c}{f'_{c,0}}}$	30
	Malvar and Ross [16]	3×10^{-6}	1.016	0.333	$\log\beta = 6\delta - 2$	$\delta = \frac{1}{1 + 8\frac{f'_c}{f'_{c,0}}}$	1
	New best fitting model	3×10^{-6}	5.535	–	–	$\delta = \frac{1}{1 + 8\frac{f'_c}{f'_{c,0}}}$	1×10^{-5}

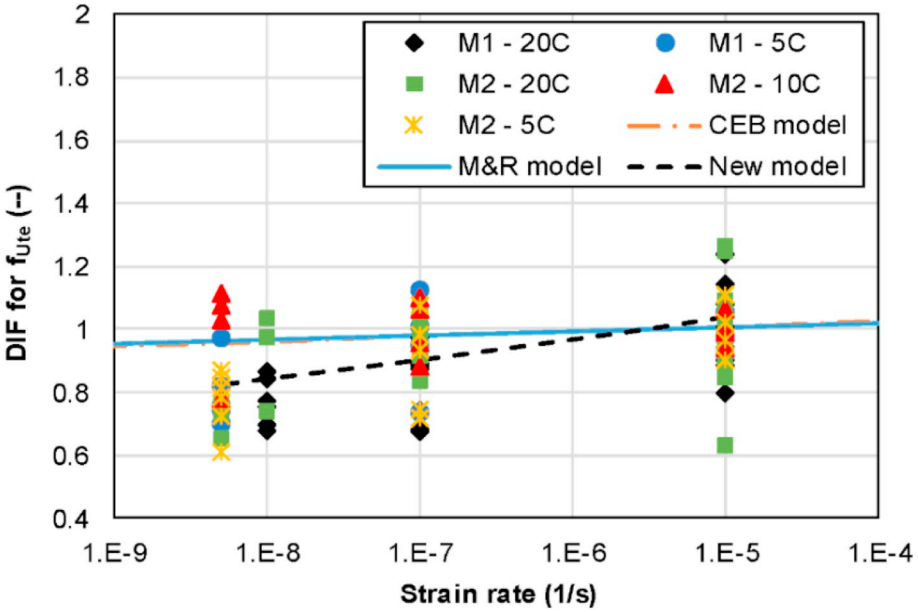

Fig. 18. DIF for elastic limit of Mix I and II at very low loading rates, along with the predictions of analytical models (M&R - Malvar and Ross).

Table 6
Parameters of the analytical models for the prediction of effect of strain rate on the DIF for ε_{Utu}.

Property	Model	$\dot{\varepsilon}_s$ (s^{-1})	A (–)	B (–)	β (–)	δ (–)	t (s^{-1})
DIFε_{Utu}	Thomas et al. [19]	3×10^{-6}	1	1.5	1.2847×10^{11}	8.26×10^{-3}	20
	Park et al. [23]	3×10^{-6}	1	0.3286	0.003998	0.01465	25
	New best fitting model	3×10^{-6}	−9.925	–	–	$\delta = \frac{1}{1+8\frac{f'_c}{f'_{c,0}}}$	1×10^{-5}

domain on ε_{Utu} for UHPFRC [23–25,31–33,35]. All these studies were compiled by Thomas et al. [19] and a model for DIF was proposed similar to Eq. (2). A similar model was also proposed by Park et al. [23] for the trend of ε_{Utu}. The parameters of both models are shown in Table 6.

Fig. 19 shows the predictions of the Thomas model and the Park model at very low strain rates, along with the test results in the present study. It can be seen that the general predictions of the models, is a decrease in ε_{Utu} with a decrease in the strain rate, which is in contrast to the findings of the present study. As such, a new best fitting model for the test results was proposed, as seen in Table 6, which is also shown in Fig. 19 for strain rates $< 1 \times 10^{-5}$ s^{-1}. However, more test results are needed at very low strain rates to confirm the validity of this model.

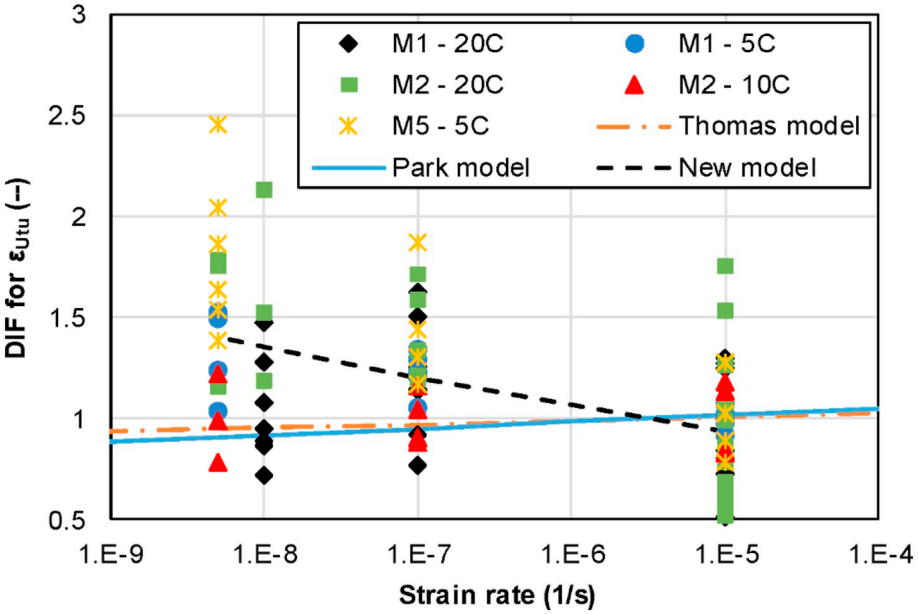

Fig. 19. DIF for strain at tensile strength of Mix I and II at very low loading rates, along with the predictions of analytical models.

5. Conclusions

- Uniaxial tensile tests were performed at different loading rates from quasi-static to very low, for two types of mixes; Mix I with pure type I cement and silica fume and Mix II with silica fume and 50% replacement of type I cement with limestone filler, under three different curing temperatures; 20 °C, 10 °C and 5 °C. The tests at strain rates $< 1 \times 10^{-6}\ s^{-1}$ were the first of their kind for UHPFRC materials.

- Effect of strain rate
  - o The elastic limit was found to decrease considerably with the decrease in the strain rate. At very low loading rates, the elastic limit showed a drop of 19%–28% when compared to that at quasi-static strain rates. The results are even more interesting for softening UHPFRC or less robust SH-UHPFRC.
  - o Acoustic emission measurements on uniaxial tensile tests confirmed the validity of the inverse analysis procedure used for the determination of the elastic limit in tension.
  - o The elastic modulus in tension was found to be insensitive to the varying strain rates.
  - o The tensile strength was also found to be insensitive to the strain rates at strain rates $< 1 \times 10^{-6}\ s^{-1}$. It was concluded that the strain rate insensitivity of tensile strength at very low strain rates, could be either because of the strain rate insensitivity of the fiber pullout at these loading rates, or because of the factors like fiber grouping and fiber orientation which offset the intrinsic rate sensitivity.
  - o The strain at tensile strength increased as the strain rate decreased. It was attributed to the fact that even at lower strain rates, when the f_{Ute} is lower, the fibrous mix remains the same and therefore becomes more efficient in achieving strain hardening.
- Effect of temperature
  - o The elastic limit and tensile strength were both found to increase with a decrease in curing temperature, which was attributed to the formation of denser microstructure with lesser quantities and sizes of capillary pores, and a better fiber matrix bond at lower temperatures.
  - o The strain at tensile strength was found to be insensitive to the curing temperature.
- Analytical modelling
  - o Existing DIF models for f_{Ute} in the dynamic domain of strain rate were extended to the very low strain rate domain and the predictions were compared. A new best fitting model for strain rates $< 1 \times 10^{-5}\ s^{-1}$ was proposed. The results could be used for the development of new guidelines for serviceability for UHPFRC materials.
  - o A new best fitting model was developed to predict the trend of ε_{Utu}, which requires further validation using test results.

CRediT authorship contribution statement

Mohamed Abdul Hafiz: Methodology, Validation, Formal Analysis, Investigation, Writing – Original Draft, Writing – Review & Editing, Visualization, Project Administration. **Emmanuel Denarié:** Conceptualization, Methodology, Formal Analysis, Resources, Writing – Review & Editing, Visualization, Supervision, Project administration, Funding Acquisition.

Acknowledgements

The project was financially supported by the Swiss National Science Foundation (grant 200021_153394/1). The authors would like to gratefully acknowledge the help given by the technicians of GIC-ENAC-EPFL Mr. S. Despont, Mr. G. Guignet and Mr. S. Demierre and Mr. A. Hajiesmaeili in performing the experimental works in the laboratory. Mix II was developed by Mr. A. Hajiesmaeili.

Declaration of competing interest

We confirm that there are no conflicts of interest between the different authors regarding the contents presented in the research.

References

[1] E. Denarié, E. Brühwiler, Cast-on site UHPFRC for improvement of existing structures – achievements over the last 10 years in practice and research, in: high perform, Fiber Reinf. Cem. Compos. 7 (2015) 473–480.
[2] Comité Euro-International du Béton, CEB-FIP Model Code 1990, Trowbridge, Wiltshire, UK, 1993.
[3] H. Rüsch, Research toward a general flexural theory for structural concrete, ACI J. 57 (1960) 1–28.
[4] H.W. Reinhardt, H.A.W. Cornelissen, Zeitstandzugversuche an Beton, Baustoffe, Bauverlag, Wiesbad, 1985, pp. 162–167.
[5] F.P. Zhou, Time Dependent Crack Growth and Fracture in Concrete, Doctoral Thesis, Report TVBM-1011 Division of Building Materials, Lund Institute of Technology, Sweden, 1992.
[6] A.E. Hansen, Time Dependent Tensile Fracture of Concrete, (1991).
[7] H.A. Körmeling, Strain Rate and Temperature Behaviour of Steel Fiber Concrete in Tension, Doctoral Thesis Delft University of Technology, 1986.
[8] P.Y.T.N.C. Allen Ross, J.W. Tedesco, Split-Hopkinson pressure-bar tests on concrete and mortar in tension and compression, Mater. J. 86 (1989) 475–481, https://doi.org/10.14359/2065.
[9] J.W. Tedesco, C.A. Ross, P.B. McGill, B.P. O'Neil, Numerical analysis of high strain rate concrete direct tension tests, Comput. Struct. 40 (1991) 313–327, https://doi.org/10.1016/0045-7949(91)90357-R.
[10] F.M. Mellinger, D.L. Birkimer, Measurement of Stress and Strain on Cylindrical Test Specimens of Rock and Concrete under Impact Loading, (1966).
[11] R. John, T. Antoun, A.M. Rajendran, Effect of strain rate and size on tensile strength of concrete, Shock Compression Condens. Matter–1991, 1992, pp. 501–504, , https://doi.org/10.1016/B978-0-444-89732-9.50115-1.
[12] A.J. Zielinski, H.W. Reinhard, H.A. Körmeling, Experiments on concrete under repeated uniaxial impact tensile loading, Mater. Constr. 14 (1981) 163–169, https://doi.org/10.1007/BF02473920.
[13] W.L. Cowell, Dynamic Properties of Plain Portland Cement Concrete, Naval Civil Engineering Laboratory, Port Hueneme, CA, 1966.
[14] J. Takeda, H. Tachikawa, Deformation and fracture of concrete subjected to dynamic load, Proc. Int. Conf. Mech. Behav. Mater. V, 1971 , Kyoto, Japan.
[15] O.P. Kvirikadze, Determination of the ultimate strength and modulus of deformation of concrete at different rates of loading, Int. Symp. Test. Situ Concr. Struct., Budapest, Hungary, 1977, pp. 109–117.
[16] L.J. M, C.A. Ross, Review of strain rate effects for concrete in tension, Mater. J. 95 (1998) 735–739, https://doi.org/10.14359/418.
[17] J.W.T.C. Allen Ross, Steven T. Kuennen, Effects of strain rate on concrete strength, Mater. J. 92 (1995) 37–45, https://doi.org/10.14359/1175.
[18] D. Tasevski, M.F. Ruiz, A. Muttoni, Compressive strength and deformation capacity of concrete under sustained loading and low stress rates, J. Adv. Concr. Technol. 16 (2018) 396–415, https://doi.org/10.3151/jact.16.396.
[19] R.J. Thomas, A.D. Sorensen, Review of strain rate effects for UHPC in tension, Constr. Build. Mater. 153 (2017) 846–856, https://doi.org/10.1016/J.CONBUILDMAT.2017.07.168.
[20] K. Fujikake, T. Senga, N. Ueda, T. Ohno, M. Katagiri, Effects of strain rate on tensile behavior of reactive powder concrete, J. Adv. Concr. Technol. 4 (2006) 79–84, https://doi.org/10.3151/jact.4.79.
[21] P.R. Edouard Parant Eric Jacquelin, Claude Boulay, Strain rate effect on bending behavior of new ultra-high-performance cement-based composite, Mater. J. 104 (2007), https://doi.org/10.14359/18901.
[22] E. Cadoni, D. Forni, Experimental analysis of the UHPFRCs behavior under tension at high stress rate, Eur. Phys. J. Spec. Top. 225 (2016) 253–264, https://doi.org/10.1140/epjst/e2016-02639-2.
[23] S.H. Park, D.J. Kim, S.W. Kim, Investigating the impact resistance of ultra-high-performance fiber-reinforced concrete using an improved strain energy impact test machine, Constr. Build. Mater. 125 (2016) 145–159, https://doi.org/10.1016/J.CONBUILDMAT.2016.08.027.
[24] J.K. Park, S.-W. Kim, D.J. Kim, Matrix-strength-dependent strain-rate sensitivity of strain-hardening fiber-reinforced cementitious composites under tensile impact, Compos. Struct. 162 (2017) 313–324, https://doi.org/10.1016/J.COMPSTRUCT.2016.12.022.
[25] N.T. Tran, D.J. Kim, Synergistic response of blending fibers in ultra-high-performance concrete under high rate tensile loads, Cem. Concr. Compos. 78 (2017) 132–145, https://doi.org/10.1016/J.CEMCONCOMP.2017.01.008.
[26] A.M. Soliman, M.L. Nehdi, Effect of partially hydrated cementitious materials and superabsorbent polymer on early-age shrinkage of UHPC, Constr. Build. Mater. 41 (2013) 270–275, https://doi.org/10.1016/J.CONBUILDMAT.2012.12.008.
[27] Y. Su, J. Li, C. Wu, P. Wu, Z.-X. Li, Effects of steel fibres on dynamic strength of UHPC, Constr. Build. Mater. 114 (2016) 708–718, https://doi.org/10.1016/J.CONBUILDMAT.2016.04.007.
[28] Y. Su, J. Li, C. Wu, P. Wu, Z.-X. Li, Influences of nano-particles on dynamic strength of ultra-high performance concrete, Compos. Part B Eng. 91 (2016) 595–609, https://doi.org/10.1016/J.COMPOSITESB.2016.01.044.

[29] M. Nöldgen, W. Riedel, K. Thoma, E. Fehling, Properties of ultra high performance concrete (UHPC) in tension at high strain rates, VIII Int. Conf. Fract. Mech. Concr. Concr. Struct, 2013.
[30] S.G. Millard, T.C.K. Molyneaux, S.J. Barnett, X. Gao, Dynamic enhancement of blast-resistant ultra high performance fibre-reinforced concrete under flexural and shear loading, Int. J. Impact Eng. 37 (2010) 405–413, https://doi.org/10.1016/J.IJIMPENG.2009.09.004.
[31] N.T. Tran, T.K. Tran, D.J. Kim, High rate response of ultra-high-performance fiber-reinforced concretes under direct tension, Cem. Concr. Res. 69 (2015) 72–87, https://doi.org/10.1016/J.CEMCONRES.2014.12.008.
[32] S. Pyo, K. Wille, S. El-Tawil, A.E. Naaman, Strain rate dependent properties of ultra high performance fiber reinforced concrete (UHP-FRC) under tension, Cem. Concr. Compos. 56 (2015) 15–24, https://doi.org/10.1016/J.CEMCONCOMP.2014.10.002.
[33] R. Ranade, V.C. Li, W.F. Heard, Tensile rate effects in high strength-high ductility concrete, Cem. Concr. Res. 68 (2015) 94–104, https://doi.org/10.1016/J.CEMCONRES.2014.11.005.
[34] M. Xu, K. Wille, Fracture energy of UHP-FRC under direct tensile loading applied at low strain rates, Compos. Part B Eng. 80 (2015) 116–125, https://doi.org/10.1016/J.COMPOSITESB.2015.05.031.
[35] S. Pyo, S. El-Tawil, A.E. Naaman, Direct tensile behavior of ultra high performance fiber reinforced concrete (UHP-FRC) at high strain rates, Cem. Concr. Res. 88 (2016) 144–156, https://doi.org/10.1016/J.CEMCONRES.2016.07.003.
[36] K. Wille, M. Xu, S. El-Tawil, A.E. Naaman, Dynamic impact factors of strain hardening UHP-FRC under direct tensile loading at low strain rates, Mater. Struct. 49 (2016) 1351–1365, https://doi.org/10.1617/s11527-015-0581-y.
[37] Z.P. Bazant, S. Prasannan, Solidification theory for concrete creep. I: formulation, J. Eng. Mech. 115 (1989) 1691–1703.
[38] Z.P. Bažant, S. Prasannan, Solidification theory for concrete creep: I: verification and application, ASCE J. Eng. Mech. 115 (1989) 1704–1725.
[39] P. Rossi, N. Godart, J.L. Robert, J.P. Gervais, D. Bruhat, Investigation of the basic creep of concrete by acoustic emission, Proceedings, Creep Shrinkage Concr, 1993, pp. 33–38.
[40] Z.P. Bažant, R. Gettu, Rate effects and load relaxation in static fracture of concrete, ACI Mater. J. 89 (1992) 456–468.
[41] E. Denarié, Etude experimentale des couplages Viscoelasticite - Croissance des fissures dans les betons de ciment, Doctoral thesis No: 2195 Ecole Polytechnique Fédérale de Lausanne, 2000.
[42] A. Switek-Rey, E. Denarié, E. Brühwiler, Early age creep and relaxation of UHPFRC under low to high tensile stresses, Cem. Concr. Res. 83 (2016) 57–69.
[43] A.E. Switek, Time-Dependent Response of Ultra High Performance Fibre Reinforced Concrete (UHPFRC) under Low to High Tensile Stresses, Doctoral thesis No: 4899 Ecole Polytechnique Fédérale de Lausanne, Switzerland, 2011.
[44] A. Kamen, Comportement au jeune âge et différé d'un BFUP écrouissant sous les effets thermomécaniques, Doctoral thesis No: 3827 Ecole Polytechnique Fédérale de Lausanne, Switzerland, 2007.
[45] A. Kamen, E. Denarié, H. Sadouki, E. Brühwiler, Evaluation of UHPFRC activation energy using empirical models, Mater. Struct. 42 (2009) 527–537, https://doi.org/10.1617/s11527-008-9400-z.
[46] M. Kazemi Kamyab, Autogenous Shrinkage and Hydration Kinetics of SH-UHPFRC under Moderate to Low Temperature Curing Conditions, Doctoral thesis No: 5681 Ecole Polytechnique Fédérale de Lausanne, Switzerland, 2013.
[47] V.Y. Garas, K.E. Kurtis, L.F. Kahn, Creep of UHPC in tension and compression: effect of thermal treatment, Cem. Concr. Compos. 34 (2012) 493–502, https://doi.org/10.1016/J.CEMCONCOMP.2011.12.002.
[48] W. Li, Z. Huang, G. Hu, W. Hui Duan, S.P. Shah, Early-age shrinkage development of ultra-high-performance concrete under heat curing treatment, Constr. Build. Mater. 131 (2017) 767–774, https://doi.org/10.1016/J.CONBUILDMAT.2016.11.024.
[49] V.Y. Garas, A.R. Jayapalan, L.F. Kahn, K.E. Kurtis, Micro- and nanoscale characterization of effect of interfacial transition zone on tensile creep of ultra-high-performance concrete, Transp. Res. Rec. 2141 (2010) 82–88, https://doi.org/10.3141/2141-14.
[50] V.Y. Garas, L.F. Kahn, K.E. Kurtis, Short-term tensile creep and shrinkage of ultra-high performance concrete, Cem. Concr. Compos. 31 (2009) 147–152.
[51] A. Kamen, E. Denarié, E. Brühwiler, Thermal effects on physico-mechanical properties of ultra-high-performance fiber-reinforced concrete, ACI Mater. J. 104 (2007) 415–423.
[52] A. Kamen, E. Denarié, H. Sadouki, E. Brühwiler, Thermo-mechanical response of UHPFRC at early age — Experimental study and numerical simulation, Cem. Concr. Res. 38 (2008) 822–831, https://doi.org/10.1016/J.CEMCONRES.2008.01.009.
[53] H. Yiğiter, S. Aydın, H. Yazıcı, M.Y. Yardımcı, Mechanical performance of low cement reactive powder concrete (LCRPC), Compos. Part B Eng. 43 (2012) 2907–2914, https://doi.org/10.1016/J.COMPOSITESB.2012.07.042.
[54] P.R. Prem, B.H. Bharatkumar, N.R. Iyer, Influence of curing regimes on compressive strength of ultra high performance concrete, Sadhana 38 (2013) 1421–1431, https://doi.org/10.1007/s12046-013-0159-8.
[55] T. (Tess) M. Ahlborn, D.K. Harris, D.L. Misson, E.J. Peuse, Characterization of strength and durability of ultra-high-performance concrete under variable curing conditions, Transp. Res. Rec. 2251 (2011) 68–75, https://doi.org/10.3141/2251-07.
[56] W. Huang, H. Kazemi-Kamyab, W. Sun, K. Scrivener, Effect of cement substitution by limestone on the hydration and microstructural development of ultra-high performance concrete (UHPC), Cem. Concr. Compos. 77 (2017) 86–101.
[57] N. Mahasenan, S. Smith, K. Humphreys, The cement industry and global climate change: current and potential future cement industry CO2 emissions, Greenh. Gas Control Technol. - 6th Int. Conf, 2003, pp. 995–1000, , https://doi.org/10.1016/B978-008044276-1/50157-4.
[58] M.A. Nisbet, M.L. Marceau, M.G. VanGeem, Environmental Life Cycle Inventory of Portland Cement Concrete, (2002).
[59] P. Rossi, A. Arca, E. Parant, P. Fakhri, Bending and compressive behaviours of a new cement composite, Cem. Concr. Res. 35 (2005) 27–33, https://doi.org/10.1016/J.CEMCONRES.2004.05.043.
[60] E. Denarié, Recommendations for the Tailoring of UHPFRC Recipes for Rehabilitation, Deliverable ARCHES D06, http://arches.fehrl.org, (2009).
[61] E. Denarié, K. Habel, J. Wuest, SAMARIS Deliverable D13, Report on Preliminary Studies for the Use of HPFRCC for the Rehabilitation of Road Infrastructure Components, http://samaris.zag.si, (2004).
[62] M.A. Hafiz, A. Hajiesmaeili, E. Denarié, Tensile Response of Low Clinker UHPFRC Subjected to Fully Restrained Shrinkage, Submitted to Cement and Concrete Research, January (2019).
[63] M.A. Hafiz, E. Denarié, Experimental study of tensile response of strain hardening UHPFRC at early age, Strain-Hardening Cem. Compos, Springer, Dresden, Germany, 2018, pp. 308–315.
[64] A. Switek-Rey, E. Denarié, E. Brühwiler, Tensile creep of UHPFRC under low and high stresses, 4th Int. Conf. Constr. Mater. – Performance, Innov. Struct. Implic., Nagoya, Japan, 2009, pp. 432–437.
[65] T. Kanakubo, Tensile characteristics evaluation method for ductile fiber-reinforced cementitious composites, J. Adv. Concr. Technol. 4 (2006) 3–17, https://doi.org/10.3151/jact.4.3.
[66] H. Neuber, Der zugbeanspruchte flachstab mit optimalem querschnittsubergang, Forsch. Im Ingenieurwes. 35 (1969) 29–30.
[67] S.-T. Kang, J.-I. Choi, K.-T. Koh, K.S. Lee, B.Y. Lee, Hybrid effects of steel fiber and microfiber on the tensile behavior of ultra-high performance concrete, Compos. Struct. 145 (2016) 37–42, https://doi.org/10.1016/J.COMPSTRUCT.2016.02.075.
[68] SIA, Cahier Technique 2052, Béton fibré ultra-performant (BFUP): Matériaux, dimensionnement et exécution, SIA, Zürich, 2017, p. 2017.
[69] E. Denarié, "Recommendations for the Improvement of Annexes D and E of SIA CT 2052", Private Communication to Prof. Dr. Cornelius Oesterlee (Bern University of Applied Sciences, Also Chair of SIA CT 2052 Committee), Email from E. Denarié from 6.12.2016, (2016).
[70] M.K. McVay, Spall Damage of Concrete Structures, (1988).
[71] D. joo Kim, S. El-Tawil, A.E. Naaman, Rate-dependent tensile behavior of high performance fiber reinforced cementitious composites, Mater. Struct. 42 (2009) 399–414, https://doi.org/10.1617/s11527-008-9390-x.
[72] C.A. Ross, J.W. Tedesco, M.L. Hughes, D.M. Jerome, Moisture and strain rate effects on concrete strength, ACI Mater. J. 93 (1996) 293–300, https://doi.org/10.14359/9814.
[73] H.W. Reinhardt, P. Rossi, J.G.M. van Mier, Joint investigation of concrete at high rates of loading, Mater. Struct. 23 (1990) 213–216, https://doi.org/10.1007/BF02473020.
[74] P. Rossi, F. Toutlemonde, Effect of loading rate on the tensile behaviour of concrete: description of the physical mechanisms, Mater. Struct. 29 (1996) 116, https://doi.org/10.1007/BF02486201.
[75] D. Yan, G. Lin, Dynamic properties of concrete in direct tension, Cem. Concr. Res. 36 (2006) 1371–1378, https://doi.org/10.1016/J.CEMCONRES.2006.03.003.
[76] A.E. Naaman, Engineered steel fibers with optimal properties for reinforcement of cement composites, J. Adv. Concr. Technol. 1 (2003) 241–252, https://doi.org/10.3151/jact.1.241.
[77] M. Xu, B. Hallinan, K. Wille, Effect of loading rates on pullout behavior of high strength steel fibers embedded in ultra-high performance concrete, Cem. Concr. Compos. 70 (2016) 98–109, https://doi.org/10.1016/J.CEMCONCOMP.2016.03.014.
[78] D.J. Kim, S. El-Tawil, A.E. Naaman, Loading rate effect on pullout behavior of deformed steel fibers, ACI Mater. J. 105 (2008) 576–584.
[79] Y.-S. Tai, S. El-Tawil, T.-H. Chung, Performance of deformed steel fibers embedded in ultra-high performance concrete subjected to various pullout rates, Cem. Concr. Res. 89 (2016) 1–13, https://doi.org/10.1016/J.CEMCONRES.2016.07.013.
[80] Y.-S. Tai, S. El-Tawil, High loading-rate pullout behavior of inclined deformed steel fibers embedded in ultra-high performance concrete, Constr. Build. Mater. 148 (2017) 204–218, https://doi.org/10.1016/J.CONBUILDMAT.2017.05.018.
[81] K.S. Douglas, S.L. Billington, Strain rate dependence of HPFRCC cylinders in monotonic tension, Mater. Struct. 44 (2011) 391–404.
[82] E. Yang, V.C. Li, Rate dependence in engineered cementitious composites, in: Int. RILEM work. High perform, Fiber Reinf. Cem. Compos. Struct. Appl, RILEM Publications SARL, 2006, pp. 83–92.
[83] E. Gallucci, X. Zhang, K.L. Scrivener, Effect of temperature on the microstructure of calcium silicate hydrate (C-S-H), Cem. Concr. Res. 53 (2013) 185–195, https://doi.org/10.1016/j.cemconres.2013.06.008.
[84] N. Banthia, J.-F. Trottier, Effects of curing temperature and early freezing on the pull-out behavior of steel fibres, Cem. Concr. Res. 19 (1989) 400–410, https://doi.org/10.1016/0008-8846(89)90029-X.
[85] H. Mihashi, F.H. Wittmann, Stochastic approach to study the influence of rate of loading on strength of concrete, HERON 25 (1980) 1–55.